iVES OENO One vine & wine

DOI: https://doi.org/10.20870/oeno-one.2026.60.2.9840

OPEN ACCESS

VITICULTURE ORIGINAL RESEARCH ARTICLES

Evaluating early detection of grapevine trunk diseases from asymptomatic leaves based on hyperspectral imagery

Israel Jiménez Luna[1], Renaud Travadon[1], Paula Jacqueline Eschen[2], Kendra Baumgartner[2,*]

[1] Department of Plant Pathology, University of California, Davis, CA 95616, USA
[2] United States Department of Agriculture- Agricultural Research Service, Crops Pathology and Genetics Research Unit, Davis, CA 95616, USA

Article number: 9840

*correspondence: grapes@nextvintageconsulting.com

Associate editor: Luca Brillante

Received: 07 January 2026

Accepted: 21 May 2026

Published: 16 June 2026

This article is published under the **Creative Commons licence** (CC BY 4.0).

Use of all or part of the content of this article must mention the authors, the year of publication, the title, the name of the journal, the volume, the pages and the DOI in compliance with the information given above.

ABSTRACT

Horticultural crops propagated vegetatively are at risk of infections by vascular pathogens, which are transmitted from infected cuttings. In grapevine nurseries, plants contaminated by fungi that cause grapevine trunk disease are widely documented. Detection of trunk diseases in the nursery could be an efficient approach to prevent their spread to vineyards. Early detection, however, is confounded by a delay of up to a year before visual symptoms appear. This incubation period exceeds the 6 to 8 months grapevines are grown in the nursery; visual inspection for leaf symptoms is thus not a means of detection. We evaluated hyperspectral imagery as a non-destructive alternative. Host responses (anatomical, physiological, transcriptomic) have been documented within weeks of infection. Such responses may be associated with changes in hyperspectral reflectance of asymptomatic leaves. For 14 weeks, we compared hyperspectral reflectance (410 to 1000 nm) of asymptomatic leaves on potted grapevines, the woody stems of which were either inoculated with fungi that cause trunk diseases Botryosphaeria dieback (*Neofusicoccum parvum*) and Esca (*Phaeomoniella chlamydospora* and *Tropicoporus texanus*), are were non-inoculated (controls). Destructive sampling of woody stems, at weeks 2, 8, and 14, revealed the largest internal wood lesions in *N. parvum*-inoculated plants. Normalised difference spectral indices (NDSIs) revealed spectral shifts among inoculated plants, for example, in the VIS spectrum (*e.g.*, 670 nm) and at the 'red edge' (700–730 nm), at weeks 8 and 9. However, separate Principal Component Analyses (PCAs) of the VIS and NIR spectra, at weeks 8, 9, and 14, revealed high within-treatment variation among samples and PERMANOVA was not significant. Further, partial least-squares discriminant analyses (PLS-DAs), under a 2-class model, distinguished leaves of control plants versus each inoculation treatment with low to moderate discriminant accuracies of 55 to 79 %. High variation among plants within a treatment may have been due to some leaves having connections via the vascular network with infected cells in the woody stem, whereas other leaves did not. Further research under nursery conditions and for a longer incubation period may achieve higher discriminant accuracies between infected plants and healthy plants, to substantiate the prospects of hyperspectral imaging as an early detection tool for grapevine trunk diseases.

KEYWORDS: Botryosphaeria dieback, Esca, fungal diseases, machine learning, non-destructive detection, optical sensor, *Vitis vinifera*

INTRODUCTION

Trunk diseases affect most California vineyards and, when unmanaged, they negatively impact the long-term productivity of *Vitis vinifera* cultivars of wine grapes (Kaplan *et al.*, 2016) and table grapes (Baumgartner *et al.*, 2019). The causal fungi are genetically diverse, including species that span four Classes across the Fungal Divisions Ascomycota and Basidiomycota (Lawrence *et al.*, 2017). Among grapevine diseases, trunk diseases are particularly detrimental because the fungal pathogens cause chronic infections of the permanent, woody structure of the vine. A wood infection located at the base of a fruiting position will permanently impact the growth and yield of distal shoots. Symptoms range from stunted shoot growth and death of fruiting positions ('dieback' caused by Botryosphaeria-, Eutypa-, and Phomopsis diebacks) to spotted fruit ('measles' caused by Esca) (Figure 1). With limited options for curative management of trunk diseases, short of cutting off the entire top of the vine and retraining a new shoot from the base of the trunk (Baumgartner *et al.*, 2024), early-detection tools are needed to help identify contaminated plants before symptoms appear and trunk diseases spread. Early-detection tools for trunk diseases, as part of a phytosanitary program in the nursery, would help minimise the establishment of young vineyards with contaminated nursery stock.

Visual diagnosis of diseases caused by pathogens that internally infect the wood of horticultural crops, such as bacterial canker of kiwi, for example, which is caused by the bacterium *Pseudomonas syringae* pv *actinidiae* (Renzi *et al.*, 2012), is often confounded by a long delay between infection and symptom expression. Disease symptoms may be visibly similar to those of abiotic stress, as is the case for Laurel wilt of avocado (Ploetz *et al.*, 2012), or there may be an uneven distribution of the pathogen in the leaf canopy, as is the case for Verticillium wilt of olive (Jiménez-Díaz *et al.*, 2012).

In the case of trunk diseases, early detection is confounded by the slow-developing leaf symptoms (Figure 1). Depending on the virulence of the pathogen and the susceptibility of the cultivar, it can take a year or more between the time of wood infection and the first appearance of obvious external symptoms. Plants propagated in the nursery, for a single growing season of 6–8 months, are thus unlikely to develop leaf symptoms before delivery of nursery stock to growers. Current diagnostic methods require the collection of wood samples, whereby the internal wood symptoms are revealed by cutting through the woody stem (Figure 1). To confirm exactly which pathogen is causing the wood symptoms, pieces of symptomatic wood are then collected for culture-based or DNA-based detection



FIGURE 1. Symptoms of grapevine trunk diseases: Botryosphaeria dieback and Esca.

Botryosphaeria dieback kills shoots (A), which grow out from infected fruiting positions. Esca causes a discoloration (red and/or yellow) and scorched areas of the leaf blades, in between the veins and at the margins (B). Fruit on shoots with these leaf symptoms of Esca becomes spotted (C) and does not ripen or develop properly. The wood symptom of Botryosphaeria dieback is a wood canker (D). The wood symptoms of Esca include dark brown to black spots, which are sometimes distributed in concentric rings in cross-section through infected wood (E), and a white rot-type of wood decay (F).

(*e.g.*, macroarray (Úrbez-Torres *et al.*, 2015)). This approach is destructive and time-consuming; thus, it is not practical for screening nursery plants at a commercial scale.

Nursery stock that is free of disease ('clean nursery stock') is a critical component of grapevine health. California grapevine nurseries, which participate in the California Department of Food and Agriculture's certification program, must use certified, virus-free plants to establish the vineyards from which they will gather vegetative cuttings each year (CDFA, 2016). The certified virus-free plants are available from a 'foundation block' (*e.g.*, Foundation Plant Services, University of California, Davis, USA). Foundation blocks are regularly screened (per the certification-program guidelines) for a set of over a dozen viruses.

Science has advanced our knowledge of which grapevine pathogens, in addition to viruses, originate in the nursery. The fungal pathogens that cause the trunk diseases Botryosphaeria dieback, Esca, Eutypa dieback, and Phomopsis dieback have been detected in California nursery stock (Garcia *et al.*, 2025). Infections of nursery stock by some of the same pathogens are also documented from grape-growing regions around the world (Akgül *et al.*, 2023; Carbone *et al.*, 2022; Gramaje *et al.*, 2018; Hrycan *et al.*, 2023; van Jaarsveld *et al.*, 2025). Such findings suggest that contaminated nursery stock is one possible source of inoculum in new vineyards (Fischer, 2019). However, work is still needed to identify the relative importance of contamination at the stages of nursery propagation (Waite *et al.*, 2018). Spores may land on the surface of dormant canes of 'mother vines', from which cuttings of the canes are collected for scions and rootstocks, and then spores may be distributed from contaminated cuttings to healthy cuttings, when grouped together into hydration tanks or callus medium (Gramaje & Armengol, 2011). Fungal mycelium that colonises cuttings, and thus remains in a newly grafted plant ('benchgraft'), is subsequently planted in a new vineyard (Waite *et al.*, 2018). In addition, the graft union may serve as an infection court for infection by spores during the time that benchgrafts are rooted in nursery soil (Pouzoulet *et al.*, 2013b). Because California nursery stock is distributed to many grape-growing regions, contaminated nursery stock is potentially a concern across the US. Rapid and reliable disease diagnostics, for screening asymptomatic vines in the nursery for trunk diseases, would improve the phytosanitary quality of nursery stock.

Hyperspectral imaging of leaves has been evaluated as a study tool to monitor plant stress or to detect crop diseases (Al-Saddik *et al.*, 2018; Gold *et al.*, 2020a; Wei *et al.*, 2021). This non-destructive approach reveals biophysical and/or biochemical changes in plant leaves, based on the intensity of light reflected across a whole spectral region (hyperspectral) or at specific spectral bands (multispectral), depending on the camera (Bendel *et al.*, 2020). Hyperspectral imaging of asymptomatic leaves has been examined as a means of early detection of viruses, namely Grapevine red blotch virus (Laroche-Pinel *et al.*, 2025) and Grapevine leafroll-associated viruses (Gao *et al.*, 2020), infecting the vine's woody tissues. Hyperspectral patterns distinguishing asymptomatic from symptomatic vines are reported in vineyards with Esca (Al-Saddik *et al.*, 2018; Bendel *et al.*, 2020; Calamita *et al.*, 2021; Junges *et al.*, 2020). These studies were conducted in the field and distinguished vines with advanced, visible symptoms, but the potential for hyperspectral imaging for early detection (before symptoms are visible) remains to be demonstrated. Further, because the causal pathogens often cause mixed infections within a vine (*e.g.*, Dekrey *et al.*, 2022; Travadon *et al.*, 2022), the specificity of the hyperspectral-reflectance patterns to Esca, and not to other trunk diseases, is not known.

Despite the complexities of the trunk-disease study system (*e.g.*, mixed infections, slow-developing leaf symptoms, lack of assays to reliably reproduce leaf symptoms), there are reports in the literature of host responses that occur within weeks of infection, as demonstrated after greenhouse inoculations with the causal pathogens (Table 1). We identified two widespread trunk diseases (Botryosphaeria dieback and Esca) and a set of three pathogens (*Neofusicoccum parvum*, causal species of Botryosphaeria dieback; *Phaeomoniella chlamydospora* and *Tropicoporus texanus*, causal species of Esca) that we hypothesised were likely to induce contrasting changes in hyperspectral reflectance in asymptomatic leaves. These pathogens all colonise xylem vessels (Czemmel *et al.*, 2015; Pouzoulet *et al.*, 2013a), but they cause different symptoms (Figure 1). *Neofusicoccum parvum* damages plant cells by enzymatic decomposition of the wood, causing a soft rot-type of wood decay (Galarneau *et al.*, 2025). Fungal toxins secreted by *P. chlamydospora* are thought to be associated with the unique leaf and fruit symptoms (Bruno *et al.*, 2007). In addition to the direct effects of infection on plant cells by fungal enzymes and/or toxins, we expect hyperspectral reflectance of the leaves to be associated with host responses to infection, which are unique to the different diseases (*e.g.*, vessel occlusions in the leaf midrib, associated with Esca (Bortolami *et al.*, 2023)). The host responses to infection cannot be conveniently measured in the nursery as a means of diagnosing trunk diseases. However, designing an experiment to encompass a time frame during which such host responses occur provided an opportunity for us to determine whether a technique like hyperspectral imagery, which can be conveniently measured in the nursery, is sufficient for diagnosing trunk diseases.

MATERIALS AND METHODS

1. Greenhouse inoculations

Dormant cuttings were made from dormant canes of grapevines of table grape *Vitis vinifera* 'Thompson Seedless' clone 1, trimmed to a consistent length (~20 cm) of one to two nodes, and soaked in water overnight. Cuttings were then callused in a mixture of perlite and vermiculite (1:1, vol/vol), at 30 °C and 85 % humidity for 21 days. Once root and shoot initials emerged, callused cuttings were coated in melted paraffin wax (Gulf Wax; Royal Oak Enterprises, Roswell, GA, USA) to prevent moisture loss, and potted in 2-L pots with sterile potting mix, amended with redwood

TABLE 1. Characteristics during grapevine infection by Botryosphaeria-dieback pathogen *Neofusicoccum parvum*, and Esca pathogens *Phaeomoniella chlamydospora* and *Tropicoporus texanus*.

Fungal species	Characteristics of infection	Reference
Neofusicoccum parvum (Division Ascomycota, Class Dothideomycetes, Order Botryosphaeriales, Family Botryosphaeriaceae)		
	Damage to plant cells	
	Causes shoots, growing distal to the inoculated woody stem, to wilt and die on some plants, at 12 weeks post-inoculation.	(Czemmel *et al.*, 2015)
	Colonises xylem fibers, xylem vessels, xylem rays, phloem, periderm, and pith.	(Czemmel *et al.*, 2015)
	Produces fungal toxins mellein, isosclerone, and tyrosol *in vitro*.	(Evidente *et al.*, 2010)
	Enzymatically degrades cellulose, hemicellulose, and lignin, causing a soft rot-type of wood decay.	(Galarneau *et al.*, 2025)
	Host response to infection	
	During infection, starch is depleted from xylem fibers and rays.	(Czemmel *et al.*, 2015)
	During infection, xylem vessels become occluded.	(Czemmel *et al.*, 2015)
	During infection, grape genes upregulated in woody stems include those associated with pathogenesis-related proteins, total phenolics, flavonoids, and stilbenes.	(Massonnet *et al.*, 2017)
Phaeomoniella chlamydospora (Division Ascomycota, Class Eurotiomycetes, Order Chaetotyriales, Family Herpotrichiellaceae)		
	Damage to plant cells	
	Produces fungal toxins isosclerone and scytalone i*n vitro* and *in planta*.	(Bruno *et al.*, 2007)
	Colonises xylem fibres, xylem vessels, xylem rays, phloem, periderm, and pith.	(Pouzoulet *et al.*, 2013a)
	Host response to infection	
	During infection, xylem vessels become occluded.	(Pouzoulet *et al.*, 2013a)
Tropicoporus texanus (Division Basidiomycota, Class Agaricomycotina, Order Hymenochaetales, Family Hymenochaetacaeae)		
	Damage to plant cells	
	Causes leaves on shoots, growing distal to the inoculated woody stem, to scorch on some plants, at 1 year post-inoculation.	(Brown *et al.*, 2020)
	Genome sequence contains genes similar to those of white-rot fungi.	(Garcia *et al.*, 2024)

bark and slow-release fertiliser (Osmocote Pro 24-4-9, Scotts, Marysville, OH, USA). Potted grapevines were grown under greenhouse conditions [natural sunlight photoperiod of approx. 14 h per day, 25 ± 1 °C (day), 18 ± 3 °C (night)] for 8 months before inoculation, with irrigation three times per week and fertilisation once per week. During the 1-year-period the plants were in the greenhouse (from February 2021 to January 2022, with the inoculation treatments starting in October 2021), they were trained to one main shoot, which was trimmed to approximately 1 m in length. Plants did not flower or fruit.

Inoculation treatments were a control treatment of non-inoculated wounded plants (controls) and plants inoculated with one of three fungi: *N. parvum* isolate UCD646So (Úrbez-Torres *et al.*, 2006), *P. chlamydospora* isolate C25 (Rooney-Latham, 2005) and *T. texanus* isolate TX09 (Brown *et al.*, 2020). For each of these four treatments, there were 40 replicate plants per treatment (4 plants for weekly hyperspectral imaging + 36 plants for destructive sampling, to measure lesion lengths at 2, 8, and 14 weeks post-inoculation) and an additional 5 replicate plants for destructive sampling before inoculation. Inoculum of *N. parvum* consisted of 4-mm-diameter agar plugs colonised by vegetative mycelium, taken from 4-day cultures on potato dextrose agar (PDA; Difco Laboratories, Detroit, MI, USA). For *P. chlamydospora* and *T. texanus*, mycelial plugs were taken from 2-week-old PDA cultures. A power drill was used to wound the woody stem (wound of 4 mm diameter by 3 mm depth), approx. 2 cm below and aligned with the uppermost node, and then a 4-mm agar plug (from the PDA cultures for inoculated plants, from non-colonised PDA for control plants) was set into the wound, which was immediately sealed with Vaseline (Unilever, Rotterdam, London, UK) and Parafilm (Bemis Co., Neenah, WI, USA), to prevent inoculum desiccation. Plants were arranged in a completely randomised design in a greenhouse (Armstrong Experiment Station, University of California, Davis). Lastly, the woody stems of five plants were destructively sampled immediately before inoculation (as described below for recovery attempts), to evaluate background levels of contaminating fungi, which may have been present in the nursery stock or due to infections that occurred during their year of growth in the greenhouse. One day later, this experiment was duplicated with a second set of PDA cultures and plants, and all plants were arranged in a completely randomised design in a second greenhouse.

No leaf symptoms were expected to develop during the 14 weeks post-inoculation, based on the results of previous greenhouse experiments with the same three pathogens, which were carried out for time scales ranging from 3 months to 1 year (Table 1). Time points of 2 and 8 weeks post-inoculation were selected for measurement of lesion lengths because these time points have been shown, in previous greenhouse experiments with *N. parvum* or *P. chlamydospora*, to be associated with significant changes in anatomical, biochemical, and/or transcriptomic responses in the grape host plant (Czemmel *et al.*, 2015; Galarneau *et al.*, 2019; Galarneau *et al.*, 2021). At 2, 8, and 14 weeks post-inoculation, 12 plants per treatment per greenhouse were destructively sampled to measure the extent of internal wood discolouration above and below the inoculation site (*i.e.*, lesion length) in the woody stem. To reveal the internal wood lesions, the green shoots, roots, and bark of each plant were removed with a flame-sterilised knife and pruning shears. The woody stems were then surface sterilised in 1 % sodium hypochlorite for 2 mins and rinsed with deionised water. The length of each stem was recorded, and then the stem was cut longitudinally, through the inoculation site, to expose the lesion (inoculated plants) or the slight discolouration around the wound site (control plants), the length of which was measured with a digital calliper.

Recovery attempts were used to confirm whether inoculated plants were infected and whether control plants were uninfected. This quality-control step was necessary to ensure that a lesion was caused by the pathogen inoculated to the plant, rather than by a contaminant pathogen. Among the plants destructively sampled at 2, 8, and 14 weeks post-inoculation, recovery was attempted by cutting 10 pieces (2 × 5 × 5 mm) of wood from the distal margin of the lesion of inoculated plants and from the wound site of control plants. Wood pieces were surface sterilised in 0.6 % sodium hypochlorite (pH 7.2) for 30 s, rinsed twice for 30 s in sterile deionised water, plated on PDA amended with tetracycline (1 mg L^{-1}), and incubated in the dark at approximately 22 °C for 14 to 21 days. Inoculated plants that did not develop an infection (*i.e.*, a lesion did not develop and the pathogen was not recovered from the inoculation site) or that were contaminated (*i.e.*, a different pathogen was recovered from the lesion margin) were removed from the data set. Control plants that were contaminated (*i.e.*, a lesion developed and/or a pathogen was recovered from the wound site) were removed from the data set.

An analysis of variance (ANOVA), using RStudio software Version 4.1.2 (downloaded 2021-11-01), was used to determine the effects of inoculation treatment (control, *N. parvum*, *P. chlamydospora*, and *T. texanus*), time point (2, 8, and 14 weeks post-inoculation), and their interaction on lesion length. Inoculation treatment and time were considered as fixed effects, with greenhouse considered as a random effect. Normality and homogeneity of variances were evaluated using normal probability plots and Levene's test. The means for significant effects ($P < 0.05$) were compared by Tukey's test.

2. Hyperspectral imaging

A visible-near infrared (VNIR) hyperspectral camera (Pika XC2, Resonon, USA), operating in the spectral range of 400 to 1000 nm, was used to measure hyperspectral reflectance of the adaxial leaf surface. The system consists of a 12-bit, line-scanner camera with a spectral resolution of 1.3 nm (capable of delivering 462 spectral bands) and a focal-length lens of 23 mm. All images were acquired using SpectrononPro (version 3.4.0, Resonon, USA). Images were taken at 0700–1100 h, from plants removed temporarily from the greenhouses, brought inside the headhouse, and placed inside

a photobooth with artificial lighting (Figure S1), thereby shielding the leaves from shadowing and external lighting, the latter of which can saturate hyperspectral-image quality (Manea & Calin, 2015). The camera was stationary on top of a stage, which was operated by an automated, rotating motor that moved across the field of view of each leaf.

The same plants were imaged each week (four plants per treatment × four treatments × two greenhouses = 32 plants total). The following criteria were used to select leaves of similar maturity: shoot positions between the fifth and seventh node, growth stage of full expansion (when photosynthetic pigment content is expected to be maximal), and of similar size (approximately 8 cm length × 10 cm width). A different set of three leaves was imaged per plant per week. The average normalised spectrum was then derived from the three leaves per plant per timepoint. Hyperspectral-image cubes were 1600 pixels × n × 462 pixels, where n was the number of line scans used to generate each data cube. The plants imaged weekly were destructively harvested at the end of the experiment, for measurement of week 14 lesion lengths (for inclusion with lesion lengths that were measured among the 12 plants per treatment per greenhouse) and to confirm whether inoculated plants were infected and control plants were uninfected. This latter quality-control step was necessary to ensure that hyperspectral responses of the leaves were associated with the internal wood infection. Inoculated plants that did not develop an infection (*i.e.*, a lesion did not develop and the pathogen was not recovered from the inoculation site) or that were contaminated (*i.e.*, a different pathogen was recovered from the lesion margin) were removed from the dataset. Control plants that were contaminated (*i.e.*, a pathogen was recovered from the wound site) were removed from the data set.

Corrected average reflectance (R) was calculated using Spectronon Pro (version 3.4.0, Resonon, USA), with weekly dark calibration (image taken with the lens cap on and the lights off) and white calibration (image taken of a white Teflon sheet). R was calculated from the raw spectral reflectance (R0) as follows: R = R0–D/W–D (Ariana *et al.*, 2006; Tahmasbian *et al.*, 2017), where D and W represent dark noise and white reflectance, respectively. The preprocessing steps of hyperspectral images were as follows: i) conversion from raw images to radiance, and ii) conversion from radiance to reflectance. The mean spectral signature was calculated by selecting the entire leaf area. Data were exported as .txt files.

For every image (*i.e.*, on a per-leaf basis), the spectral range was 394 to 1010 nm. However, due to signal instability at either extreme of this range (< 410 nm and > 1000 nm), reflectance values from 410 to 1000 nm were analysed. Detection and removal of outliers (namely, abnormal reflectance values due to measurement error) were based on the interquartile range of a given reflectance value among those of all leaves. To mitigate the effect on the signal-to-noise ratio, spectra were 'smoothed' using a 25-window point Savitzky–Golay method and a sixth-order polynomial transformation (Ruffin & King, 1999). For each week, spectral curves were plotted of reflectance values at each wavelength (averaged among the three leaves per plant per treatment). Visual comparison of spectral curves at each week was used as a basis to select hyperspectral reflectance values for further analyses, specifically for weeks when spectral curves had a standard shape and when there were visible differences in the curves among treatments. Hyperspectral reflectance, at weeks at which spectral curves had a standard shape (*i.e.*, consistent with that of vegetation), was considered for further analyses, namely calculation of vegetation indices, partial least squares discriminant analysis (PLS-DA), and multivariate analyses [Principal Component Analysis (PCA), Permutational Multivariate Analysis of Variance (PERMANOVA)]. The standard shape of a spectral curve was defined as showing a general trend of low reflectance values for wavelengths in the visible (VIS) range and higher reflectance values for wavelengths in the near infrared (NIR) range. Because chlorophyll is the dominant pigment of vegetation during the growing season, it absorbs the vast majority of solar radiation in the visible range, hence low reflectance values. Higher reflectance values at wavelengths in the NIR range reflect lower absorption of light. Among weeks when spectral curves of each treatment had a standard shape, a second criterion for further analyses was obvious differences in the VIS and/or NIR ranges in reflectance among treatments (*i.e.*, the curves not overlapping).

3. Vegetation indices

For weeks at which spectral curves had a standard shape for all treatments and were visibly different among treatments, a total of 28 vegetation indices were calculated per plant (Table S1), and then were compared among all four treatments, using ANOVAs to examine the effect of treatment on the index values. Moreover, for each inoculation treatment, normalised difference spectral indices [NDSIs, Equation (1)] were calculated for all possible combinations of wavelengths (from 410 to 1000 nm), as follows:

$$NDSI\,[i, j] = (R_i - R_j) / (R_i + R_j) \qquad \text{Equation (1)}$$

where R_i = intensity of reflected light at wavelength$_i$, and R_j = intensity of reflected light at wavelength$_j$. NDSIs were then compared between control plants and each set of inoculated plants (*N. parvum*, *P. chlamydospora*, or *T. texanus*) for the same pairs of wavelengths, within a time point. The strength of the relationship between NDSIs of control plants versus those of each set of inoculated plants (in pairwise comparisons, within a time point) was evaluated based on Pearson's Correlation Coefficients, which were then illustrated as heat maps, to visualise NDSIs that differed most. Correlations were considered significant at $P < 0.05$. All analyses were conducted in R, using the *tidyverse* package (Wickham *et al.*, 2019).

4. Partial least squares discriminant analysis

A supervised machine learning algorithm called partial least squares discriminant analysis (PLS-DA) (Gold *et al.*, 2020b; Junges *et al.*, 2020; Pérez Roncal *et al.*, 2022) was used to classify inoculation treatments based on hyperspectral reflectance at 410 to 1000 nm (averaged across all seven

plants per treatment), using R packages *caret* (Kuhn, 2015) and *pls* (Mevik & Wehrens, 2015). This approach maximises covariance between the independent Y variables (inoculation treatments) and the dependent X variables (spectral matrix) to identify wavelengths that differ most between treatments (PLS components) (Gold *et al.*, 2020a; Gromski *et al.*, 2015). PLS-DA algorithms were examined at different weeks as follows: four-class classifiers (control, *N. parvum*, *P. chlamydospora*, *T. texanus*), and two-class classifiers for pairwise comparisons between control plants versus each set of inoculated plants (*N. parvum*, *P. chlamydospora*, or *T. texanus*). PLS-DA analyses were permuted 100 times by dividing 70 % of the observations ($n = 5$ plants per treatment) into training (calibration) and 30 % of the observations ($n = 2$ plants per treatment) into testing (cross-validation). To prevent over-fitting of the model, internal cross-validation was performed by identifying the ideal number of latent vectors and examining the predicted residual error sum of squares (PRESS) (Gold *et al.*, 2020a; Gold *et al.*, 2020b). We selected the number of latent vectors with the lowest PRESS across all permutations. Then, discriminating wavelengths were identified by obtaining and ranking the absolute value of averaged standardised coefficients across 100 simulations. Classification accuracy was based on Cohen's kappa values (κ) (Rosenfield & Fitzpatrick-Lins, 1986), which range from –1 (no agreement between true and predicted classifications) to +1 (perfect agreement between true and predicted classifications). A finer scale of interpretation of classification accuracy, also based on κ values, is as follows (Landis & Koch, 1977): –1.00 to 0 (poor), 0 to 0.20 (slight), 0.21 to 0.40 (fair), 0.41 to 0.60 (moderate), 0.61 to 0.80 (substantial), and 0.81 to 1.00 (almost perfect).

5. Multivariate analyses

Principal component analysis (PCA) was used to examine the effects of inoculation treatment on hyperspectral reflectance. Reflectance values from 410 to 1000 nm, averaged across all replicate plants per treatment, were first converted to Euclidean distances, as calculated with the R package *factoextra* (Kassambara & Mundt, 2020). Principal components that accounted for the highest percentage of variation among samples were visualised in treatment-sample bi-plots, showing the locations of treatment centroids relative to each plant sample. Separate analyses were conducted for each week. The semiparametric method Permutational Multivariate Analysis of Variance (PERMANOVA) was used to determine whether spectral-reflectance differences among inoculation treatments were statistically significant (based on pseudo F and corresponding P values), with R package *vegan* (Oksanen *et al.*, 2015). Reflectance values from 410 to 1000 nm, averaged across all seven plants per treatment, were first converted to Euclidean distances.

RESULTS

Mean lesion lengths varied significantly among inoculation treatments at all three time points at which plants were destructively sampled for lesion lengths (2, 8, and 14 weeks post-inoculation), based on the results of ANOVA ($P < 0.05$). Starting at 2 weeks post-inoculation, mean lesion lengths of plants inoculated with *N. parvum* were significantly larger than those of control plants, the latter of which were consistently below 10 mm at all three time points (Figure 2). Starting at 8 weeks post-inoculation, mean lesion lengths of plants inoculated with *P. chlamydospora* or *T. texanus* were significantly larger than that of control plants. At all three time points, plants inoculated with *N. parvum* had the largest lesions, which were twice that of plants inoculated with *P. chlamydospora* or *T. texanus* at 2 weeks post-inoculation. No plants developed leaf symptoms throughout the experiment. Among the 24 replicate plants per treatment (summed across two greenhouses), three sets of which were destructively harvested at 2, 8, and 14 weeks post-inoculation, one to three plants per treatment were found to be either contaminated by a different pathogen or did not develop an internal wood infection. These contaminated and non-infected plants were removed from the lesion-length data sets at 2, 8, and 14 weeks. Among the eight replicate plants per treatment (summed across two greenhouses), the leaves of which were imaged weekly, one plant per treatment was found to be either contaminated by a different pathogen or did not develop an internal wood infection. These contaminated and non-infected plants were removed from the lesion-length data set at week 14 and from the entire hyperspectral dataset, resulting in a uniform sample size of seven replicate plants per treatment for analyses of hyperspectral reflectance.

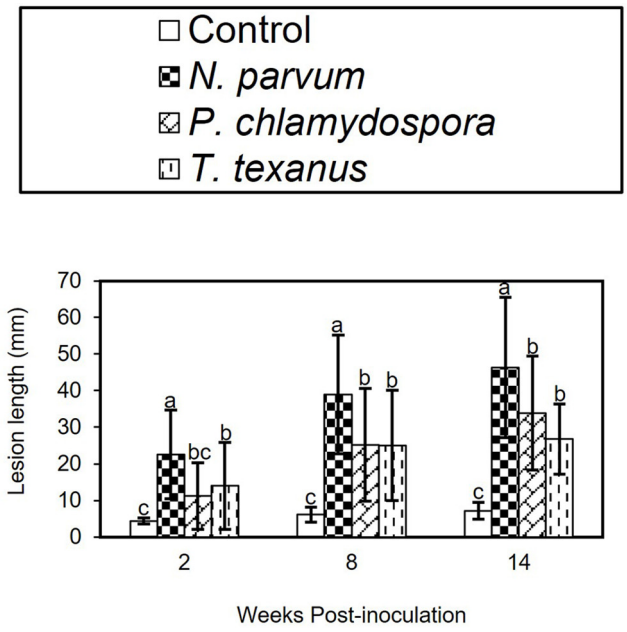


FIGURE 2. Mean length of internal lesions in the woody stems of potted *Vitis vinifera* 'Thompson Seedless'.

Each column represents the mean of $n = 21$ to 23 replicate plants at each of weeks 2 and 8, and $n = 28$ to 30 replicate plants at week 14. Error bars represent standard deviations. Means that are significantly different among inoculation treatments within a timepoint are represented by different letters at the tops of the columns (Tukey's test; $P \leq 0.05$).

The spectral curves for weeks 8, 9, and 14 were consistent with the standard shape of a spectral-reflection curve of vegetation, and there were visible differences among treatments in the VIS and/or NIR spectra (Figure 3). At week 8, there was separation among the curves for all four treatments at 725–775 nm; at 900–1000 nm, *N. parvum* had higher reflectance than all other treatments (Figure 3A). At week 9, there was separation among the curves for all four treatments at 750–800 nm; at 825–875 nm, the control and *N. parvum* had higher reflectance than *P. chlamydospora* and *T. texanus* (Figure 3B). At week 14, there were two pairs of spectral curves; the spectral curves for the control and *T. texanus* overlapped, and those of *N. parvum* and *P. chlamydospora* overlapped, throughout much of the VIS and NIR spectra (Figure 3C). *Neofusicoccum parvum* and *P. chlamydospora* had higher reflectance than the control and *T. texanus* at 425–650 nm and 725–1000 nm. Nonetheless, in spite of visual separation of the spectral curves at some wavelengths, differences in mean reflectance among treatments were not statistically significant, based on PERMANOVA, at 8, 9, or 14 weeks post-inoculation (*data not shown*).

NDSIs revealed spectral shifts in reflectance patterns from the leaves of plants inoculated with the three pathogens, based on correlation coefficients of NDSIs (displayed in heatmaps; Figure 4). At week 8, leaves had some similar patterns of NDSIs that were strongly associated with all three pathogens, including an interaction of the 'red edge' (700–730 nm) with chlorophyll *a* (670 nm) and interactions of 750–800 nm with the entire NIR spectrum (Figure 4A–C). Different patterns of NDSIs at week 8 included a strong association of the 'green edge' (520 nm) with *P. chlamydospora* (Figure 4B), and chlorophyll *b* and *a* (650 and 670 nm, respectively) with *T. texanus* (Figure 4C). Persisting from week 8 to week 9, for all three pathogens, was the interaction of the 'red edge' (700–730 nm) with chlorophyll *a* (670 nm; Figure 4D–F). At week 9, there were more numerous and stronger differences in NDSIs between control versus inoculated plants, including interactions of the 'red edge' with narrow bands of the VIS spectrum and interactions of the beginning of the NIR spectrum (800–900 nm) with the entire NIR spectrum (Figure 4D–F). Different patterns of NDSIs at week 9 included a strong association of the 'green edge' (520 nm) with *N. parvum* (Figure 4D) and *P. chlamydospora* (Figure 4E), and interactions of the beginning of the NIR spectrum (800–900 nm) with the entire NIR spectrum for *T. texanus* (Figure 4F). At week 14, there were strong associations of narrow VIS bands interacting with the VIS and NIR spectra for *N. parvum* and *P. chlamydospora* (Figure 4G–H). NDSIs of the control were more similar to *T. texanus* (*i.e.*, with low correlation coefficients for the same NDSIs; Figure 4I) at week 14, in comparison. Among all 28 vegetation indices calculated at weeks 8, 9, and 14 (Figure S1), ANOVAs did not detect significant differences between control plants and inoculated plants (*data not shown*).

Hyperspectral reflectance of the NIR spectrum was separated among treatments primarily by two principal components, PC1 and PC2, which explained a combined total of 75.8 to 94.9 % of the variation, depending on the week (Figure 5A–C). High variation among samples within treatments, however, contributed to high overlap of treatment ellipses, especially at weeks 8 and 9 (Figure 5A–B). At week 14, NIR spectra of *N. parvum* and *P. chlamydospora* were similar, based on the proximity of their treatment centroids to each other and overlap of their samples to the top of the *y*-axis (PC2) (Figure 5C). Hyperspectral reflectance of the VIS spectrum was separated among treatments primarily by PC1 (which explained 78.1 to 93.5 % of the variation), with a relatively low contribution by PC2 (which explained 3.7 to 15.3 % of the variation; Figure 5D–F). Hyperspectral reflectance of the VIS spectrum was highly variable among samples within each treatment, with no separation of treatment ellipses.

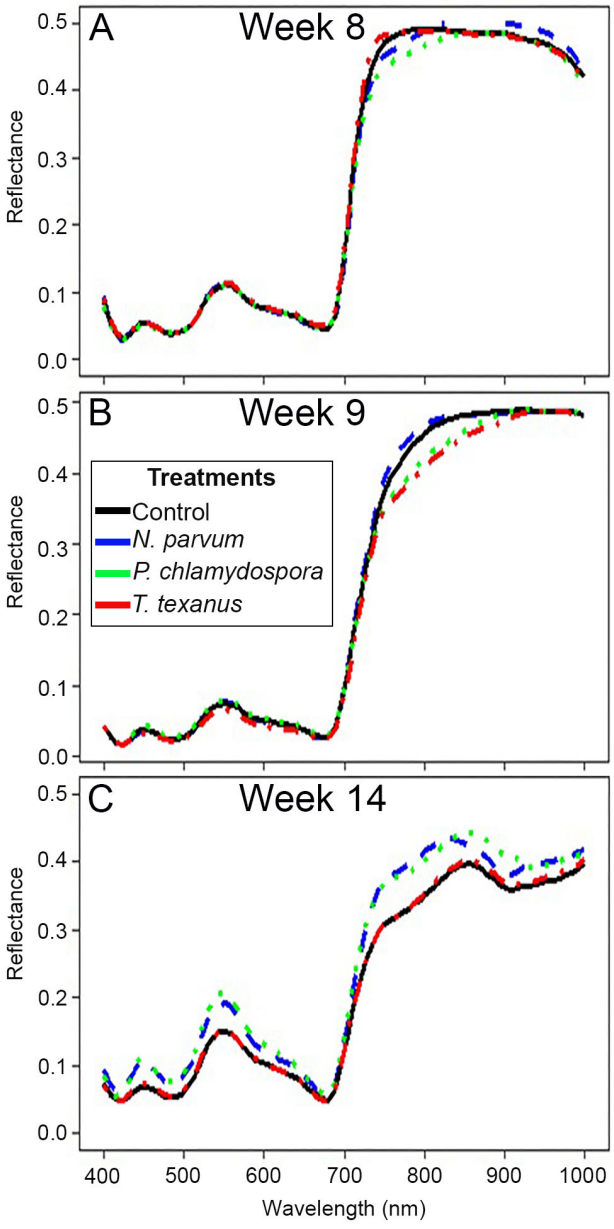


FIGURE 3. Average hyperspectral reflectance of leaves on plants in four inoculation treatments (Control, N. parvum, P. chlamydospora, T. texanus). Each line is the average of three leaves on each of seven plants per treatment, at week 8 (A), week 9 (B), and week 14 (C).

When the accuracy of classification of hyperspectral reflectance (410–1000 nm) among all four inoculation treatments (control, *N. parvum*, *P. chlamydospora*, and *T. texanus*) was evaluated at weeks 8, 9, and 14, PLS-DA mean classification accuracies ranged from a low of 49.5 % (kappa = 0.33) at week 9 to a high of 60.6 % (kappa = 0.47) at week 8 (Table 2). When the classification of hyperspectral reflectance (410–1000 nm) was evaluated in pairwise comparisons of control plants versus plants inoculated with each pathogen, cross-validation accuracies were more moderate, ranging from 61.0 to 79.0 % at week 8, 56.5 to 73.3 % at week 9, and 55.0 to 72.6 % at week 13 (Table 3). Control and *N. parvum* plants could be differentiated with the highest accuracy at week 8 (79.0 %, kappa = 0.59; Table 3), with discriminating wavelengths in the NIR spectrum (774–887 nm), which also corresponded to NDSIs that had a strong association with *N. parvum* (Figure 4A). Control and *T. texanus* plants could be differentiated with the highest accuracy at week 9 (73.3 %, kappa = 0.47; Table 3). Control and *P. chlamydospora* plants could be differentiated with the highest accuracy at week 14 (72.6 %, kappa = 0.44; Table 3).

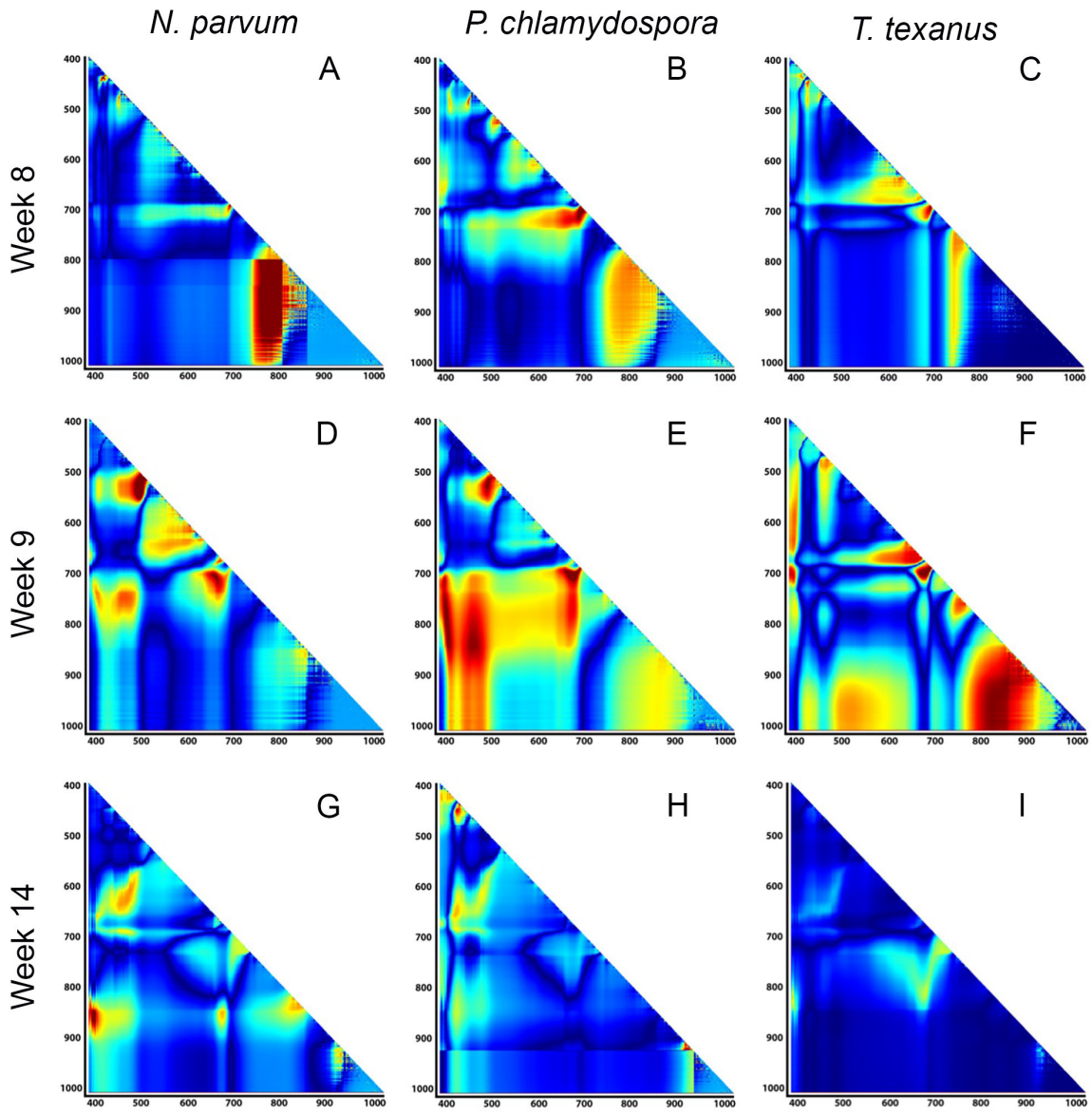


FIGURE 4. Heat maps of Pearson correlation coefficients (*r*) between normalised difference spectral indices (NDSIs) of control plants versus inoculated plants (*N. parvum, P. chlamydospora*, or *T. texanus*). The *x*- and *y*-axes represent the two wavelengths used to calculate a given NDSI. Dark blue represents no difference in NDSIs between control plants and inoculated plants (*r* = 1), whereas red represents NDSIs that varied most (*r* close to 0).

DISCUSSION

Our study is unique in investigating hyperspectral reflectance of vines inoculated under controlled conditions with individual pathogens that cause grapevine trunk diseases. In contrast, the mixed infections that typically characterise trunk diseases in the vineyard (Travadon *et al.*, 2016) could make it difficult to pinpoint disease-specific reflectance patterns. Our greenhouse experiment allowed us to test the effects of individual pathogens. NDSIs identified spectral shifts in hyperspectral reflectance of asymptomatic leaves of inoculated plants, compared to control plants, at some weeks. However, such shifts were not validated as a means of accurately differentiating inoculation treatments, given that PCAs revealed high within-treatment variability, low to moderate PLS-DA accuracies, and no significant differences in mean reflectance, based on PERMANOVA. Our findings of no significant differences among spectral curves and low accuracies (and low kappa values) based on PLS-DA are consistent with Bendel *et al.* (2020), who found that 'pre-symptomatic' leaves on vines with Esca were not distinguished from healthy leaves on healthy vines in a vineyard. In our greenhouse experiment, hyperspectral reflectance varied between the asymptomatic leaves of inoculated plants and the healthy leaves of control plants, based on NDSIs. NDSIs that were associated with all three pathogens, in pair-wise comparisons with the control, included the interaction of the 'red edge' (700–730 nm) with chlorophyll *a* (670 nm), at weeks 8 and 9. These findings are consistent with higher reflectance at 670 and 700 nm from severely symptomatic versus moderately symptomatic leaves, on vines with Esca in a vineyard (Junges *et al.*, 2020). NDSIs that involved the interaction of the beginning of NIR (800–900 nm) with the entire NIR spectrum were associated with *N. parvum* (weeks 8, 9, and 14), *P. chlamydospora* (weeks 8 and 9), and *T. texanus* (week 9). These findings are consistent with lower reflectance at 800 nm from severely symptomatic versus asymptomatic leaves, on vines with Esca in a vineyard (Junges *et al.*, 2020).

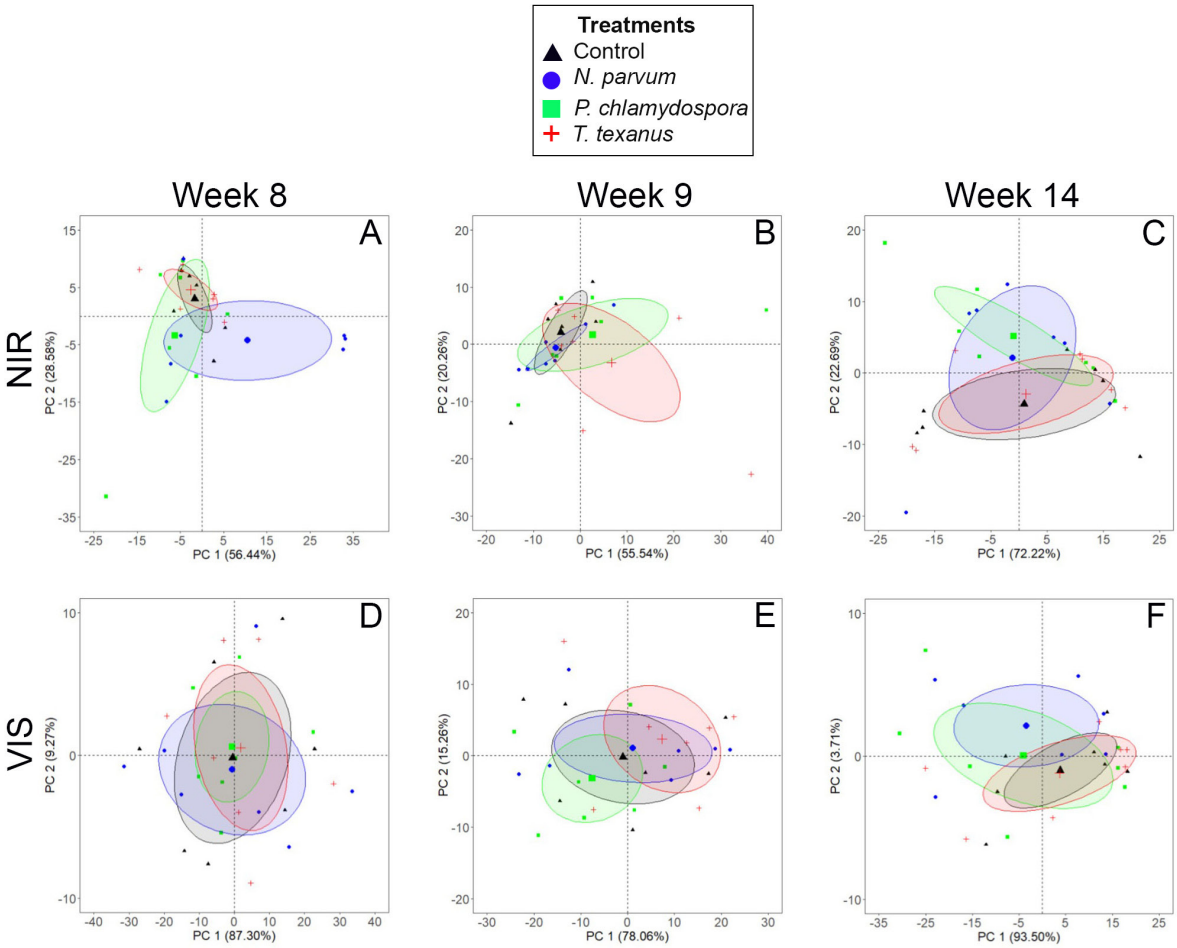


FIGURE 5. Principal component analysis (PCA) of average hyperspectral reflectance of NIR wavelengths (700 to 1000 nm) and of VIS wavelengths (410 to 700 nm), of leaves on plants in four inoculation treatments (control, *N. parvum*, *P. chlamydospora*, *T. texanus*), at 8, 9 and 14 weeks post-inoculation.

The *x*- and *y*-axes of each plot represent principal component PC1 and PC2, respectively, with the percentages of total variation that each PC accounts for shown in parentheses. Centroids for each inoculation treatment (large symbols) and their surrounding confidence ellipses ($P < 0.05$) are shown in relation to the seven replicate plants in each treatment (small symbols). Small symbols represent the average reflectance of three leaves per plant, with a different set of three fully expanded leaves per plant ($n = 7$ plants per treatment) imaged each week.

TABLE 2. Partial least squares discriminant analysis (PLS-DA) confusion matrices, in comparisons among all four inoculation treatments (*n* = 7 plants per treatment). Internal cross-validation performed with 100 permutations of a 70/30 calibration-validation data-set split (*n* = 5 plants for classification, *n* = 2 plants for validation).

Time	Comparisons				Actual # of samples per class	Producer's accuracy %
Week 8						
Kappa = 0.47						
Components = 6						
	P. chlamydospora	Control	*N. parvum*	*T. texanus*		
P. chlamydospora	3.40	1.16	0.96	1.48	7	48.57
Control	0.97	3.73	0.50	1.80	7	53.29
N. parvum	0.70	0.92	5.01	0.37	7	71.57
T. texanus	0.88	1.13	0.16	4.83	7	69.00
Total # of classified samples	5.95	6.94	6.63	8.48		
User's accuracy %	63.49	55.87	78.70	58.05		Total accuracy (Range): 60.61 % (40.61–78.27)
Week 9						
Kappa = 0.33						
Components = 4						
	P. chlamydospora	Control	*N. parvum*	*T. texanus*		
P. chlamydospora	2.82	1.41	0.90	1.87	7	40.29
Control	1.32	2.41	2.08	1.19	7	34.43
N. parvum	0.90	1.90	3.44	0.76	7	49.14
T. texanus	0.72	0.51	0.58	5.19	7	74.14
Total # of classified samples	5.76	6.23	7.00	9.01		
User's accuracy %	52.5	39.28	51.36	59.78		Total accuracy (Range): 49.50 % (30.30–68.80)
Week 14						
Kappa = 0.35						
Components = 6						
	P. chlamydospora	Control	*N. parvum*	*T. texanus*		
P. chlamydospora	3.61	0.93	1.01	1.45	7	51.57
Control	0.84	3.27	1.05	1.84	7	46.71
N. parvum	0.90	1.00	4.38	0.72	7	62.57
T. texanus	1.16	2.14	0.68	3.02	7	43.14
Total # of classified samples	6.51	7.34	7.12	7.03		
User's accuracy %	58.97	44.96	63.5	44.74		Total accuracy (Range): 51.00 % (31.70–70.10)

Although we detected statistically significant differences in NDSIs between asymptomatic leaves of inoculated plants and healthy leaves of control plants, these patterns were not sustained from week 8 and on. In a nursery, it thus may not be possible to detect such short-term changes in hyperspectral reflectance. Phenotypes of leaves did not change from asymptomatic to symptomatic during the course of our study. The lack of a greenhouse assay that reliably results in Esca symptoms is a bottleneck to the study of this trunk disease, and thus a significant limitation of our work. In the greenhouse, *P. chlamydospora* and *T. texanus* inoculations to the woody stems of potted grapevines rarely result in development of the leaf symptoms of Esca, even after a year (Brown *et al.*, 2020). In contrast, inoculations with *N. parvum* progress faster, causing a rapid wilt and collapse of shoots (*i.e.*, symptoms of Botryosphaeria dieback) by 12 weeks in some plants (Travadon *et al.*, 2013). Given this temporal difference in symptom development between Botryosphaeria dieback and Esca, we estimated that an incubation period of 14 weeks would at least allow for data collection before plants inoculated with *N. parvum* died of Botryosphaeria dieback. Even in the vineyard, variable symptom expression among years, especially regarding the leaf symptoms of Esca (Lecomte *et al.*, 2012), impacts the likelihood of leaves predictably changing from asymptomatic to symptomatic.

TABLE 3. Partial least squares discriminant analysis (PLS-DA) accuracy values and standardised coefficients, in pairwise comparisons of controls versus plants inoculated with *N. parvum, P. chlamydospora*, or *T. texanus* (*n* = 7 plants per treatment). Internal cross-validation performed with 100 permutations of a 70/30 calibration-validation data-set split (*n* = 5 plants for classification, *n* = 2 plants for validation). Most important standardised coefficients start from left to right.

		Train		Internal cross - validation			
Week	Comparison	Accuracy	Kappa	Accuracy	Kappa	Components	Top 20 standardised coefficients (nm)
8							
	Control *vs* *P. chlamydospora*	77.0 %	0.53	61.0 %	0.21	2	775, 784, 803, 778, 791, 789, 785, 797, 777, 792, 779, 786, 776, 796, 794, 793, 780, 790, 781, 774
	Control *vs* *N. parvum*	92.0 %	0.53	79.0 %	0.59	2	848, 877, 840, 886, 887, 775, 833, 853, 868, 878, 834, 847, 778, 774, 777, 829, 885, 845, 839, 776
	Control *vs* *T. texanus*	79.0 %	0.39	61.0 %	0.21	2	740, 741, 739, 742, 743, 738, 744, 737, 745, 746, 736, 747, 748, 749, 735, 750, 751, 734, 733, 752
9							
	Control *vs* *P. chlamydospora*	73.0 %	0.46	59.1 %	0.18	2	472, 473, 474, 480, 478, 483, 482, 481, 475, 484, 477, 479, 471, 485, 476, 429, 470, 486, 487, 488
	Control *vs* *N. parvum*	73.5 %	0.47	56.5 %	0.13	2	973, 924, 931, 913, 938, 921, 987, 984, 951, 936, 972, 933, 939, 925, 917, 964, 941, 935, 960, 937
	Control *vs* *T. texanus*	84.8 %	0.70	73.3 %	0.47	2	422, 417, 420, 419, 421, 423, 418, 984, 416, 987, 951, 983, 424, 413, 953, 426, 414, 974, 815, 816
14							
	Control *vs* *P. chlamydospora*	80.6 %	0.61	72.6 %	0.45	2	884, 891, 885, 886, 888, 883, 882, 889, 881, 887, 880, 890, 892, 893, 879, 894, 878, 877, 895, 876
	Control *vs* *N. parvum*	78.8 %	0.58	70.9 %	0.42	2	417, 418, 412, 419, 422, 420, 423, 424, 421, 411, 416, 410, 428, 425, 427, 429, 413, 426, 414, 415
	Control *vs* *T. texanus*	72.4 %	0.45	55.0 %	0.27	2	417, 412, 422, 418, 419, 423, 416, 420, 424, 411, 410, 413, 414, 421, 415, 668, 665, 666, 671, 667

The high variation among samples within a treatment, as reflected, especially, in PCAs of the VIS spectrum, may have been due to some leaves having connections via the vascular network with infected cells in the woody stem, whereas other leaves did not. Indeed, the symptoms of Botryosphaeria dieback and Esca are not expressed uniformly across all shoots of mature vines (Mugnai *et al.*, 1999; Úrbez-Torres, 2011). Wood symptoms of Esca are relatively localised (rather than uniform), as are connections to individual shoots via 'vascular bundles' of grapevine xylem vessels (Kassemeyer *et al.*, 2022). A longer incubation period beyond week 14 may have allowed more time for the wood infection to spread to a greater proportion of the stem, and thus to impact a greater proportion of leaves. It also may have allowed for more time to maximise the discriminant accuracies, which could potentially make this detection tool more reliable and robust. However, the incubation period of 14 weeks accommodated comparisons among the pathogens, which vary in virulence. We imaged leaves of similar age (fully expanded, between the fifth and seventh nodes) and size (approx. 8 cm length × 10 cm width) among time points. It is possible that older leaves may have different hyperspectral responses to trunk diseases than younger leaves. However, imaging older leaves, which are positioned deep within the grapevine canopy, did not seem practical for future application in a nursery. Instead, leaves that were likely to be more accessible to a hyperspectral camera, closer to the tip of the shoot and at the top of the canopy, are where we looked for differences in hyperspectral reflectance.

Beyond our greenhouse experiment, a different approach in a nursery, on plants rooted in field soil, may be more informative for evaluating hyperspectral imagery as an early-detection tool. Assuming there is such a nursery that would be comfortable revealing the vulnerabilities of its phytosanitary practices, additional assumptions required of such a study would include the presence of plants infected by one or more pathogens that cause trunk diseases, and the presence of mixed infections. Throughout the course of the growing season, hyperspectral imaging of leaves across the nursery could account for possible changes due to infections in the woody stem. At the end of the growing season, when plants are uprooted and prepared for cold storage, the woody stems of a representative sample of plants could be destructively sampled for wood symptoms and to confirm the identities of the pathogen species, as was done by Lade *et al.* (2022). Although leaves would be likely to remain asymptomatic throughout the growing season in the nursery (similar to our greenhouse experiment), this approach could test the feasibility of hyperspectral imaging in a nursery environment, which is currently a practical limitation of using this and other digital technologies (Mahlein *et al.*, 2024).

The effects of the wood infections on the hyperspectral reflectance of the leaves may differ among the three pathogens, which vary in their wood-colonisation capabilities and in production of phytotoxic metabolites, both of which impact the host. *Neofusicoccum parvum* and *T. texanus* are wood-rotting fungi (Galarneau *et al.*, 2025; Garcia *et al.*, 2024), which degrade the xylem, thereby impacting the flow of water and soil-derived nutrients from the roots to the leaves. *Phaeomoniella chlamydospora* produces phytotoxic metabolites scytalone and isosclerone (Evidente *et al.*, 2010), which have been detected in symptomatic leaves and fruit (Bruno *et al.*, 2007). *Neofusicoccum parvum* produces phytotoxic metabolites mellein and terremutin, which have been detected in symptomatic wood (Abou-Mansour *et al.*, 2015). Reports of anatomical changes (*e.g.*, formation of tyloses and gums (Czemmel *et al.*, 2015)) and biochemical changes (*e.g.*, higher stilbene concentrations (Galarneau *et al.*, 2021)) in the wood, from potted plants inoculated with *N. parvum* and *P. chlamydospora*, respectively, represent host responses to infection, which may also affect hyperspectral reflectance of the leaves. Symptomatic leaves from vines with Esca undergo anatomical changes in response to infection, as tyloses and gels form in the xylem vessels of the peripheral veins (Bortolami *et al.*, 2023). Compared to asymptomatic leaves on vines with Esca, symptomatic leaves on the same vines have fewer and smaller starch grains and lower glutathione levels (Valtaud *et al.*, 2009), and have lower net photosynthesis, stomatal conductance, and total chlorophyll content (Petit *et al.*, 2006).

For trunk diseases like Botryosphaeria dieback and Esca, exact time frames are not reported for fungal damage to woody cells, production of phytotoxic metabolites, or host responses to infection. Furthermore, estimating the time frames of such stages of pathogenesis is complicated by the fact that they progress at different rates and the leaf symptoms rarely develop in the greenhouse. As such, it is difficult to understand how such stages might correspond to differences we detect in hyperspectral reflectance over time or among pathogens. In contrast, foliar diseases of grape, such as Powdery mildew (*Erysiphe necator*) and Downy mildew (*Plasmopara viticola*), have clear timelines for sporulation and development of their symptoms/signs on leaves, relative to the formation of susceptible tissues and environmental variables favourable to sporulation, spore dispersal, and infection. Indeed, changes in hyperspectral reflectance of the leaves tend to correspond to the presence and/or severity of symptoms (*e.g.*, Powdery mildew (Knauer *et al.*, 2017), Downy mildew (Kanaley *et al.*, 2024)). That said, the predictable development of symptoms/signs of these foliar diseases of grape, coupled with the broad range of time-tested practices to manage these diseases, suggests that early detection is not a critical first step for farmers to then decide whether or not to apply a fungicide to a vineyard.

Our findings from potted grapevines in a greenhouse experiment suggest that infection by individual pathogens, which cause Esca and Botryosphaeria dieback, may not bring about detectable changes in hyperspectral reflectance of asymptomatic leaves, in the early stages of infection. Higher classification accuracies (> 80 %) may have been possible with a larger sample size, imaging of the entire canopy, a longer incubation period, or under mixed infections, for example in a vineyard environment, where leaf symptoms

of Esca become obvious between the onset of fruit ripening (veraison) and harvest. In a nursery environment, it is important to consider how hyperspectral reflectance of the leaves might interact with the effects of abiotic stress on nursery stock of grapevines. Compared to potted plants in the greenhouse, where temperatures and irrigation are controlled, plants in the nursery are more likely to suffer from drought stress, the transcriptomic changes of which in leaves are similar to those associated with *N. parvum* infection (Galarneau *et al.*, 2019). Other factors to take collectively into account in developing a new detection tool for trunk diseases are possible interactive effects on hyperspectral reflectance due to other diseases, namely graft-transmissible viruses (Leafroll disease, Red blotch disease). As with Esca, these viral diseases may be initially introduced to the vineyard via contaminated nursery stock, and then they are spread to healthy vines in vineyards where insect vectors are present. Because trunk diseases, Leafroll disease, and Red blotch disease commonly cause chronic infections of the same vines, especially as vineyards age, the possibility of unique spectral signatures in the grapevine canopy should be accounted for.

ACKNOWLEDGEMENTS

We acknowledge funding from the USDA-ARS. The contents presented are solely the responsibility of the authors and do not necessarily represent the official views or endorsement of the USDA. USDA is an equal opportunity provider and employer. Special thanks to Dr Kaitlin Gold, Dr María del Rocío Calderón Madrid, and Dr Nikita Gambhir from Cornell AgriTech in Geneva, NY, for their technical assistance with review of the proposed statistical analyses and computational advice.

REFERENCES

Abou-Mansour, E., Debieux, J.-L., Ramirez-Suero, M., Benard-Gellon, M., Magnin-Robert, M., Spagnolo, A., Chong, J., Farine, S., Bertsch, C., L'Haridon, F., Serrano, M., Fontaine, F., Rego, C., & Larignon, P. (2015). Phytotoxic metabolites from *Neofusicoccum parvum*, a pathogen of Botryosphaeria dieback of grapevine. *Phytochemistry*, *115*, 207-215. https://doi.org/10.1016/j.phytochem.2015.01.012

Akgül, D. S., Güngör Savaş, N., Yıldız, M., Bülbül, İ., & Özarslandan, M. (2023). Current status of grapevine trunk disease pathogens on asymptomatic nursery-produced grapevines in Türkiye. *Phytopathologia Mediterannea*, *62*, 151-163. https://doi.org/10.36253/phyto-14148

Al-Saddik, H., Laybros, A., Billiot, B., & Cointault, F. (2018). Using image texture and spectral reflectance analysis to detect yellowness and Esca in grapevines at leaf-level. *Remote Sensing*, *10*, 618. https://doi.org/10.3390/rs10040618

Ariana, D. P., Lu, R., & Guyer, D. E. (2006). Near-infrared hyperspectral reflectance imaging for detection of bruises on pickling cucumbers. *Computers and Electronics in Agriculture*, *53*, 60-70. https://doi.org/10.1016/j.compag.2006.04.001

Baumgartner, K., Hillis, V., Lubell, M., Norton, M., & Kaplan, J. (2019). Managing grapevine trunk diseases in California's southern San Joaquin Valley. *American Journal of Enology and Viticulture*, *70*, 267-276. https://doi.org/10.5344/ajev.2019.18075

Baumgartner, K., Jiménez-Luna, I., & Rumbaugh, A. C. (2024). Managing Esca in susceptible 'Sauvignon blanc' wine grapes through trunk renewal. *Plant Health Progress*, *25*, 372-379. https://doi.org/10.1094/PHP-01-24-0011-SC

Bendel, N., Kicherer, A., Backhaus, A., Klück, H.-C., Seiffert, U., Fischer, M., Voegele, R. T., & Töpfer, R. (2020). Evaluating the suitability of hyper-and multispectral imaging to detect foliar symptoms of the grapevine trunk disease Esca in vineyards. *Plant Methods*, *16*, 1-18. https://doi.org/10.1186/s13007-020-00685-3

Bortolami, G., Ferrer, N., Baumgartner, K., Delzon, S., Gramaje, D., Lamarque, L. J., Romanazzi, G., Gambetta, G. A., & Delmas, C. E. L. (2023). Esca grapevine disease involves leaf hydraulic failure and represents a unique premature senescence process. *Tree Physiology*, *43*, 441-451. https://doi.org/10.1093/treephys/tpac133

Brown, A. A., Lawrence, D. P., & Baumgartner, K. (2020). Role of basidiomycete fungi in the grapevine trunk disease Esca. *Plant Pathology*, *69*, 205-220. https://doi.org/10.1111/ppa.13116

Bruno, G., Sparapano, L., & Graniti, A. (2007). Effects of three Esca-associated fungi on *Vitis vinifera* L.: IV. Diffusion through the xylem of metabolites produced by two tracheiphilous fungi in the woody tissue of grapevine leads to esca-like symptoms on leaves and berries. *Physiological and Molecular Plant Pathology*, *71*(106-124). https://doi.org/10.1016/j.pmpp.2007.12.004

Calamita, F., Imran, H. A., Vescovo, L., Mekhalfi, M. L., & La Porta, N. (2021). Early identification of root rot disease by using hyperspectral reflectance: The case of pathosystem grapevine/Armillaria. *Remote Sensing*, *13*, 2436. https://doi.org/10.20944/preprints202105.0246.v1

Carbone, M. J., Gelabert, M., Moreira, V., Mondino, P., & Alaniz, S. (2022). Grapevine nursery propagation material as source of fungal trunk disease pathogens in Uruguay. *Frontiers in Fungal Biology*, *9*, 958466. https://doi.org/10.3389/ffunb.2022.958466

CDFA. (2016). Registration and Certification of Grapevines. https://doi.org/https://www.cdfa.ca.gov/plant/pe/nsc/docs/regs/ccr_3024_grapevine.pdf

Czemmel, S., Galarneau, E. R., Travadon, R., McElrone, A. J., Cramer, G. R., & Baumgartner, K. (2015). Genes expressed in grapevine leaves reveal latent wood infection by the fungal pathogen *Neofusicoccum parvum*. *PLoS One*, *10*, e0121828. https://doi.org/10.1371/journal.pone.0121828

Dekrey, D. H., Klodd, A. E., Clark, M. D., & Blanchette, R. A. (2022). Grapevine trunk diseases of cold-hardy varieties grown in Northern Midwest vineyards coincide with canker fungi and winter injury. *PLoS One*, *17*, e0269555. https://doi.org/10.1371/journal.pone.0269555

Evidente, A., Punzo, B., Andolfi, A., Cimmino, A., Melck, D., & Luque, J. (2010). Lipophilic phytotoxins produced by *Neofusicoccum parvum*, a grapevine canker agent. *Phytopathologia Mediterannea*, *49*, 74-79. https://doi.org/https://doi.org/10.14601/Phytopathol_Mediterr-5433

Fischer, M. (2019). Grapevine trunk diseases in German viticulture. III. Biodiversity and spatial distribution of fungal pathogens in rootstock mother plants and possible relation to leaf symptoms. *Vitis*, *58*, 141-149. https://doi.org/https://doi.org/10.5073/vitis.2019.58.141-149

Galarneau, E. R., Wallis, C. M., & Baumgartner, K. (2025). Biochemical characterization of wood decay and metabolization of phenolic compounds by causal fungi of grapevine trunk diseases. *PLoS One*, *20*, e0315412. https://doi.org/10.1371/journal.pone.0315412

Galarneau, E. R. A., Lawrence, D. P., Travadon, R., & Baumgartner, K. (2019). Drought exacerbates Botryosphaeria dieback symptoms in grapevines and confounds host-based molecular markers of infection by *Neofusicoccum parvum*. *Plant Disease*, *103*, 1738-1745. https://doi.org/10.1094/PDIS-09-18-1549-RE

Galarneau, E. R. A., Lawrence, D. P., Wallis, C. M., & Baumgartner, K. (2021). A comparison of the metabolomic response of grapevine to infection with ascomycete wood-infecting fungi. *Physiological and Molecular Plant Pathology*, *113*, 101596. https://doi.org/10.1016/j.pmpp.2020.101596

Gao, Z., Khot, L. R., Naidu, R. A., & Zhang, Q. (2020). Early detection of grapevine leafroll disease in a red-berried wine grape cultivar using hyperspectral imaging. *Computers and Electronics in Agriculture*, *179*, 105807. https://doi.org/10.1016/j.compag.2020.105807

Garcia, J. F., Figueroa-Balderas, R., Delmas, C. E. L., Comont, G., Baumgartner, K., & Cantu, D. (2024). Genome analysis of the esca-associated Basidiomycetes *Fomitiporia mediterranea*, *Fomitiporia polymorpha*, *Inonotus vitis*, and *Tropicoporus texanus* reveals virulence factor repertoires characteristic of white-rot fungi. *G3*, *14*, jkae189. https://doi.org/10.1093/g3journal/jkae189

Garcia, J. F., Todd, C., Rolshausen, P. E., & Cantu, D. (2025). Nursery origin and propagation stage influence the endophytic fungal communities inhabiting grapevine planting stocks. *Phytobiomes*, *9*, 287-301. https://doi.org/10.1094/PBIOMES-09-24-0090-R

Gold, K. M., Townsend, P. A., Chlus, A., Herrmann, I., Couture, J. J., Larson, E. R., & Gevens, A. J. (2020a). Hyperspectral measurements enable pre-symptomatic detection and differentiation of contrasting physiological effects of Late blight and Early blight in potato. *Remote Sensing*, *12*, 286. https://doi.org/10.3390/rs12020286

Gold, K. M., Townsend, P. A., Herrmann, I., & Gevens, A. J. (2020b). Investigating potato late blight physiological differences across potato cultivars with spectroscopy and machine learning. *Plant Science*, *295*, 110316. https://doi.org/10.1016/j.plantsci.2019.110316

Gramaje, D., & Armengol, J. (2011). Fungal trunk pathogens in the grapevine propagation process: Potential inoculum sources, detection, identification, and management strategies. *Plant Disease*, *95*, 1040-1055. https://doi.org/10.1094/PDIS-01-11-0025

Gramaje, D., Urbez-Torres, J. R., & Sosnowski, M. R. (2018). Managing grapevine trunk diseases with respect to etiology and epidemiology: Current strategies and future prospects. *Plant Disease*, *102*, 12-39. https://doi.org/10.1094/PDIS-04-17-0512-FE

Gromski, P. S., Muhamadali, H., Ellis, D. I., Xu, Y., Correa, E., Turner, M. L., & Goodacre, R. (2015). A tutorial review: Metabolomics and partial least squares-discriminant analysis–a marriage of convenience or a shotgun wedding. *Analytica Chimica Acta*, *879*, 10-23. https://doi.org/10.1016/j.aca.2015.02.012

Hrycan, J., Theilmann, J., Mahovlic, A., Boulé, J., & Úrbez-Torres, J. R. (2023). Health status of ready-to-plant grapevine nursery material in Canada regarding young vine decline fungi. *Plant Disease*, *107*, 3708-3717. https://doi.org/10.1094/PDIS-05-23-0900-SR

Jiménez-Díaz, R. M., Cirulli, M., Bubici, G., del Mar Jiménez-Gasco, M., Antoniou, P. P., & Tjamos, E. C. (2012). Verticillium wilt, a major threat to olive production: Current status and future prospects for its management. *Plant Disease*, *96*, 304-329. https://doi.org/10.1094/PDIS-06-11-0496

Junges, A. H., Almança, M. A. K., Fajardo, T. V. M., & Ducati, J. R. (2020). Leaf hyperspectral reflectance as a potential tool to detect diseases associated with vineyard decline. *Tropical Plant Pathology*, *45*, 522-533. https://doi.org/10.1007/s40858-020-00387-0

Kanaley, K., Combs, D. B., Paul, A., Jiang, Y., Bates, T., & Gold, K. M. (2024). Assessing the capacity of high-resolution commercial satellite imagery for grapevine Downy Mildew detection and surveillance in New York State. *Phytopathology*, *114*, 2536-2545. https://doi.org/10.1094/PHYTO-11-23-0432-R

Kaplan, J., Travadon, R., Cooper, M., Hillis, V., Lubell, M., & Baumgartner, K. (2016). Identifying economic hurdles to early adoption of preventative practices: The case of trunk diseases in California winegrape vineyards. *Wine Economics and Policy*, *5*, 127-141. https://doi.org/10.1016/j.wep.2016.11.001

Kassambara, A., & Mundt, F. (2020). Factoextra: Extract and visualize the results of multivariate data analyses. *R Package Version 1.0.7*. https://doi.org/https://CRAN.R-project.org/package=factoextra

Kassemeyer, H., Kluge, F., Bieler, E., Ulrich, M., Gruner, J., Fink, S., Durrenberger, M., & Fuchs, R. (2022). Trunk anatomy of asymptomatic and symptomatic grapevines provides insights into degradation patterns of wood tissues caused by Esca-associated pathogens. *Phytopathologia Mediterannea*, *61*, 451-471. https://doi.org/10.36253/phyto-13154

Knauer, U., Matros, A., Petrovic, T., Zanker, T., Scott, E. S., & Seiffert, U. (2017). Improved classification accuracy of powdery mildew infection levels of wine grapes by spatial-spectral analysis of hyperspectral images. *Plant Methods*, *13*, 1-15. https://doi.org/10.1186/s13007-017-0198-y

Kuhn, M. (2015). Caret: Classification and regression training. *Astrophysics Source Code Library*, 1505.1003. https://ui.adsabs.harvard.edu/abs/2015ascl.soft05003K

Lade, S. B., Straus, D., & Oliva, J. (2022). Variation in fungal community in grapevine nursery stock depends on nursery, variety and rootstock. *Journal of Fungi*, *8*, 47. https://doi.org/10.3390/jof8010047

Landis, J. R., & Koch, G. G. (1977). The measurement of observer agreement for categorical data. *Biometrics*, *33*, 159-174. https://doi.org/10.2307/2529310

Laroche-Pinel, E., Singh, K., Flasco, M., Cooper, M. L., Fuchs, M., & Brillante, L. (2025). Grapevine red blotch virus detection in the vineyard: Leveraging machine learning with VIS/NIR hyperspectral images for asymptomatic and symptomatic vines. *Computers and Electronics in Agriculture*, *234*, 110251. https://doi.org/10.1016/j.compag.2025.110251

Lawrence, D. P., Travadon, R., Nita, M., & Baumgartner, K. (2017). TrunkDiseaseID.org: A molecular database for fast and accurate identification of fungi commonly isolated from grapevine wood. *Crop Protection*, *102*, 110-117. https://doi.org/10.1016/j.cropro.2017.08.017

Lecomte, P., Darrieutort, G., Liminana, J. M., Comont, G., Muruamendiaraz, A., Legorburu, F. J., Choueiri, E., Jreijiri, F., El Amil, R., & Fermaud, M. (2012). New insights into Esca of grapevine: The development of foliar symptoms and their association with xylem discoloration. *Plant Disease*, *96*, 924-934. https://doi.org/10.1094/PDIS-09-11-0776-RE

Mahlein, A.-K., Arnal Barbedo, J. G., Chiang, K.-S., Del Ponte, E. M., & Bock, C. H. (2024). From detection to protection: The role of optical sensors, robots, and artificial intelligence in modern plant disease management. *Phytopathology*, *114*, 1733-1747. https://doi.org/10.1094/PHYTO-01-24-0009-PER

Manea, D., & Calin, M. A. (2015). Hyperspectral imaging in different light conditions. *The Imaging Science Journal*, *63*, 214-219. https://doi.org/10.1179/1743131X15Y.0000000001

Massonnet, M., Figueroa-Balderas, R., Galarneau, E. R. A., Miki, S., Lawrence, D. P., Sun, Q., Wallis, C. M., Baumgartner, K., & Cantu, D. (2017). *Neofusicoccum parvum* colonization of the grapevine woody stem triggers asynchronous host responses at the site of infection and in the leaves. *Frontiers in Plant Science*, *8*, 1117 https://doi.org/10.3389/fpls.2017.01117

Mevik, B.-H., & Wehrens, R. (2015). Introduction to the pls package. *Help section of the "Pls" package of R studio software*, 1-23.

Mugnai, L., Graniti, A., & Surico, G. (1999). Esca (black measles) and brown wood-streaking: Two old and elusive diseases of grapevines. *Plant Disease*, *83*, 404-418. https://doi.org/10.1094/PDIS.1999.83.5.404

Oksanen, J., Blanchet, F. G., Kindt, R., Legendre, P., Minchin, P., O'Hara, B., Simpson, G., Solymos, P., Stevens, H., & Wagner, H. (2015). Vegan: Community Ecology Package. *R Package Version 2.2-1*. https://cran.r-project.org/web/packages/vegan/vegan.pdf

Pérez Roncal, C., Arazuri Garín, S., López Molina, C., Jarén Ceballos, C., Santesteban García, G., & López Maestresalas, A. (2022). Exploring the potential of hyperspectral imaging to detect Esca disease complex in asymptomatic grapevine leaves. *Computers and Electronics in Agriculture*, *196*, 1-12. https://doi.org/10.1016/j.compag.2022.106863

Petit, A., Vaillant, N., Boulay, M., Clément, C., & Fontaine, F. (2006). Alteration of photosynthesis in grapevines affected by Esca. *Phytopathology*, *96*, 1060-1066. https://doi.org/10.1094/PHYTO-96-1060

Ploetz, R. C., Pérez-Martínez, J. M., Smith, J. A., Hughes, M., Dreaden, T. J., Inch, S. A., & Fu, Y. (2012). Responses of avocado to laurel wilt, caused by *Raffaelea lauricola*. *Plant Pathology*, *61*, 801-808. https://doi.org/10.1111/j.1365-3059.2011.02564.x

Pouzoulet, J., Jacques, A., Besson, X., Dayde, J., & Mailhac, N. (2013a). Histopathological study of response of *Vitis vinifera* cv. Cabernet Sauvignon to bark and wood injury with and without inoculation by *Phaeomoniella chlamydospora*. *Phytopathologia Mediterranea*, *52*, 313-323. https://doi.org/https://doi.org/10.14601/Phytopathol_Mediterr-12581

Pouzoulet, J., Mailhac, N., Couderc, C., Besson, X., Dayde, J., Lummerzheim, M., & Jacques, A. (2013b). A method to detect and quantify *Phaeomoniella chlamydospora* and *Phaeoacremonium aleophilum* DNA in grapevine-wood samples. *Applied Microbiology and Biotechnology*, *97*, 10163-10175. https://doi.org/10.1007/s00253-013-5299-6

Renzi, M., Copini, P., Taddei, A. R., Rossetti, A., Gallipoli, L., Mazzaglia, A., & Balestra, G. M. (2012). Bacterial canker on kiwifruit in Italy: Anatomical changes in the wood and in the primary infection sites. *Phytopathology*, *102*, 827-840. https://doi.org/10.1094/PHYTO-02-12-0019-R

Rooney-Latham, S. (2005). *Etiology, epidemiology and pathogen biology of Esca disease of grapevines in California. Ph.D. dissertation, Publ. AAT 3191148* University of California, Davis.

Rosenfield, G. H., & Fitzpatrick-Lins, K. (1986). A coefficient of agreement as a measure of thematic classification accuracy. *Photogrammetric Engineering and Remote Sensing*, *52*, 223-227.

Ruffin, C., & King, R. L. (1999). The analysis of hyperspectral data using Savitzky-Golay filtering-Theoretical basis (part 1). International Geoscience and Remote Sensing Symposium Proceedings, Hamburg, Germany. https://doi.org/10.1109/IGARSS.1999.774430

Tahmasbian, I., Xu, Z., Abdullah, K., Zhou, J., Esmaeilani, R., Nguyen, T. T. N., & Hosseini Bai, S. (2017). The potential of hyperspectral images and partial least square regression for predicting total carbon, total nitrogen and their isotope composition in forest litterfall samples. *Journal of Soils and Sediments*, *17*, 2091-2103. https://doi.org/10.1007/s11368-017-1751-z

Travadon, R., Lawrence, D. P., Moyer, M. M., Fujiyoshi, P. T., & Baumgartner, K. (2022). Fungal species associated with grapevine trunk diseases in Washington wine-grapes and California table-grapes, with novelties in the genera *Cadophora*, *Cytospora*, and *Sporocadus*. *Frontiers in Fungal Biology*, *3*, 1018140. https://doi.org/10.3389/ffunb.2022.1018140

Travadon, R., Lecomte, P., Diarra, B., Lawrence, D. P., Renault, D., Ojeda, H., Rey, P., & Baumgartner, K. (2016). Grapevine pruning systems and cultivars influence the diversity of wood-colonizing fungi. *Fungal Ecology*, *24*, 82-93. https://doi.org/10.1016/j.funeco.2016.09.003

Travadon, R., Rolshausen, P. E., Gubler, W. D., Cadle-Davidson, L., & Baumgartner, K. (2013). Susceptibility of cultivated and wild *Vitis* spp. to wood infection by fungal trunk pathogens. *Plant Disease*, *97*, 1529-1536. https://doi.org/10.1094/PDIS-05-13-0525-RE

Úrbez-Torres, J. R. (2011). The status of Botryosphaeriaceae species infecting grapevines. *Phytopathologia Mediterranea*, *50*, S5-S45. https://doi.org/https://doi.org/10.14601/Phytopathol_Mediterr-9316

Úrbez-Torres, J. R., Haag, P., Bowen, P., Lowery, T., & O›Gorman, D. T. (2015). Development of a DNA macroarray for the detection and identification of fungal pathogens causing decline of young grapevines. *Phytopathology*, *105*, 1373-1388. https://doi.org/10.1094/PHYTO-03-15-0069-R

Úrbez-Torres, J. R., Leavitt, G. M., Voegel, T. M., & Gubler, W. D. (2006). Identification and distribution of *Botryosphaeria* spp. associated with grapevine cankers in California. *Plant Disease*, *90*, 1490-1503. https://doi.org/10.1094/PD-90-1490

Valtaud, C., Foyer, C. H., Fleurat-Lessard, P., & Bourbouloux, A. (2009). Systemic effects on leaf glutathione metabolism and defence protein expression caused by esca infection in grapevines [Article]. *Functional Plant Biology*, *36*, 260-279. https://doi.org/10.1071/FP08293

van Jaarsveld, W. J., Mostert, L., Hunter, J. J., Havenga, M., van der Rijst, M., & Halleen, F. (2025). Adverse effects of grapevine trunk diseases on canes produced from infected rootstock mother blocks. *Pest Management Science*. https://doi.org/10.1002/ps.70416

Waite, H., Armengol, J., Billones-Baaijens, R., Gramaje, D., Halleen, F., Di Marco, S., & Smart, R. (2018). A protocol for the management of grapevine rootstock mother vines to reduce latent infections by grapevine trunk pathogens in cuttings. *Phytopathologia Mediterranea*, *57*, 384-398. https://doi.org/https://doi.org/10.14601/Phytopathol_Mediterr-22772

Wei, H.-E., Grafton, M., Bretherton, M., Irwin, M., & Sandoval, E. (2021). Evaluation of point hyperspectral reflectance and multivariate regression models for grapevine water status estimation. *Remote Sensing*, *13*, 3198. https://doi.org/10.3390/rs13163198

Wickham, H., Averick, M., Bryan, J., Chang, W., McGowan, L., François, R., Grolemund, G., Hayes, A., Henry, L., Hester, J., Kuhn, M., Pedersen, T., Miller, E., Bache, S., Müller, K., Ooms, J., Robinson, D., Seidel, D., Spinu, V., & Yutani, H. (2019). Welcome to the tidyverse. *Journal of Open Source Software*, *4*, 1686. https://doi.org/10.21105/joss.01686